

University of Arkansas, Fayetteville

ScholarWorks@UARK

---

Electrical Engineering Undergraduate Honors  
Theses

Electrical Engineering

---

5-2012

## A Study on the Effects of Solar Power

Jonathan Hayes

*University of Arkansas, Fayetteville*

Follow this and additional works at: <https://scholarworks.uark.edu/eleguht>



Part of the [Energy Systems Commons](#), and the [Power and Energy Commons](#)

---

### Citation

Hayes, J. (2012). A Study on the Effects of Solar Power. *Electrical Engineering Undergraduate Honors Theses* Retrieved from <https://scholarworks.uark.edu/eleguht/23>

This Thesis is brought to you for free and open access by the Electrical Engineering at ScholarWorks@UARK. It has been accepted for inclusion in Electrical Engineering Undergraduate Honors Theses by an authorized administrator of ScholarWorks@UARK. For more information, please contact [scholar@uark.edu](mailto:scholar@uark.edu), [uarepos@uark.edu](mailto:uarepos@uark.edu).

A STUDY ON THE EFFECTS OF SOLAR POWER

An Undergraduate Honors College Thesis

By

Jonathan Keith Hayes

University of Arkansas

Department of Electrical Engineering

Spring 2012

This thesis is approved.

Thesis Advisor:

---

Dr. Juan Carlos Balda

## ABSTRACT

The utilization of new and alternative energy sources, specifically solar energy, has been on the rise and will continue to grow as we attempt to diminish our use and dependency on older, nonrenewable energy sources. One of the biggest challenges involved with the use of solar energy, or renewable energy in general, is how to provide this energy for general public use. Some of the limiting factors to this are the efficiency in which solar power can be harvested and converted into usable energy, and the cost of the technology to do this. Recent technological developments have included the microinverter, which harvests dc solar power and converts it into usable ac power on a per-module basis, making the technology a viable option for those looking to benefit from solar power. However, problems arise with solar power such as photovoltaic (PV) intermittency. PV intermittency can affect the output power quality and reliability of a PV system. But, by better understanding PV intermittency, steps can be taken in order to enhance PV systems. But regardless of the effects that intermittency has on PV system output, the benefits a large scaled PV system can have on a distribution system can still be analyzed. This thesis details the work I have done as an undergraduate, which includes testing of a microinverter, collecting irradiance data and analyzing the effects that a PV system can have on the voltage regulation of a distribution system.

## ACKNOWLEDGEMENTS

I would first like to thank Dr. Juan Carlos Balda for the opportunity to work in his lab as an undergraduate student and for all of the knowledge and experience I have gained throughout my college career from him. I would also like to thank Arthur Barnes for allowing me to work with him and for guiding me through my research experience as an undergraduate student.

Next, I would like to thank all the friends I have made throughout my time at the University of Arkansas, especially those I have had the joy of working alongside with in Dr. Balda's lab.

Finally, I would like to thank my parents, Keith and Brenda, and my sister, Katy, for all of their support and encouragement over the years and for always being there for me no matter what. Last but not least, I would like to thank my girlfriend, Hannah Brunck, for staying by my side for four years and always believing in me, encouraging me, and making me laugh when I need it most.

## CHAPTER 1: TESTING OF THE ENPHASE M190 MICROINVERTER

### 1.1 INTRODUCTION

Enphase Energy is a solar energy company whose goal is to create intelligent and reliable solar energy systems that can easily be used by anyone who wants to benefit from solar energy. One of their new and innovative technologies is the microinverter, which converts dc power to ac power on a per-module basis. In an Enphase solar energy system, a microinverter is installed directly to the racking of the solar panel and is individually connected to that PV module. This per-module basis allows for maximum peak power point tracking (MPPT) for each individual PV module, which provides the maximum power available from each module to be converted. The Enphase M190 Microinverter is one of Enphase's newest microinverter models and has a maximum ac output power of 190 W. The peak power tracking dc voltage is 22 V – 40 V with a max dc input current of 10 A. The nominal ac output current is 920 mA with a nominal voltage range of 183 V – 229 V at 60 Hz. Enphase claims that this model has a peak inverter efficiency of 95.5% and a California Energy Commission (CEC) weighted efficiency of 95.0%. The power factor is stated to be greater than 0.95 lagging [1]. Once again, a major question is the efficiency of the microinverter technology. In order to justify these claims so that they can be improved upon, the efficiency of the Enphase M190 Microinverter needs to be tested. The installation of the microinverter, testing set up and procedure will be discussed, along with values to be recorded and calculated. Experimental results will then be presented, followed by conclusions and future work to be done.

## 1.2 INSTALLATION

To begin testing the efficiency of the Enphase M190 Microinverter, installation of the microinverter was completed according to the datasheet provided by Enphase. The installation schematic is shown below in Fig. 1. The M190 Microinverter is a 208 V, three-phase ac system. The ac connector cables consist of four wires, three wires are for phases a, b and c, and the fourth is for a neutral point. The three phase wires were connected to a 3-prong male electrical plug, and plugged in to a 208 V three-phase wall outlet. The neutral wire from the ac cable and the ground connection from the case of the microinverter were wired to the neutral and grounding pins of a 120 V single-phase wall outlet. These connections can be seen in Fig. 1. A protective cap was installed on the unused ac connector cable since no other microinverters are being connected to the system. For the dc side, in order to measure the dc voltage, current and power being produced, the output of the PV module was connected to a Yokogawa Power Analyzer, which was in turn connected to the two dc input wires of the microinverter.

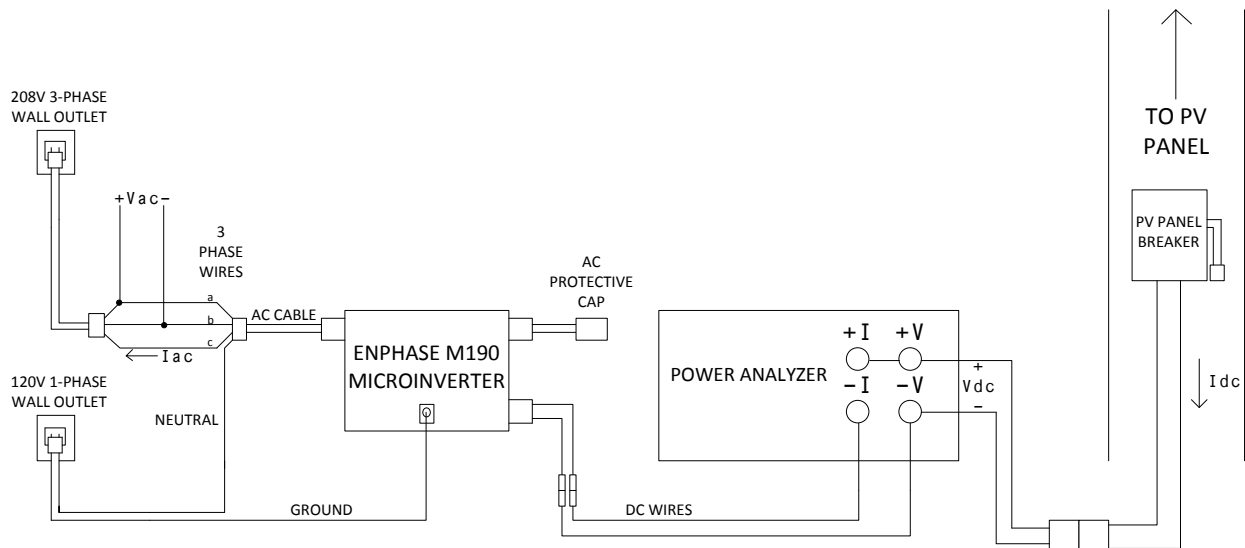


Fig. 1. Installation schematic.

### 1.3 TEST SETUP

Test setup included high voltage probes and current probes being placed in order to obtain desired quantities. On the ac side, a differential high voltage probe was set up between two phases, phase a and phase b, to measure the line-to-line voltage. A current probe was installed around one ac phase wire in order to measure the ac line current. On the dc side, in order to measure the dc voltage output of the PV module, a differential high voltage probe was connected to the +V and -V terminals of the power analyzer, as seen in Fig. 1. A current probe was installed around one of the dc input wires of the microinverter in order to measure the dc current. The voltage and current probes were connected to a Tektronix TDS 3034B oscilloscope to capture data and waveforms. The notations for all the measurements can be seen above in Fig. 1. Pictures of the microinverter and testing setup can be seen below in Fig. 2 and Fig. 3. Table I presents the equipment used during testing.





Fig. 2. Enphase M190 Microinverter.



Fig. 3. Test installation and setup.

Table I. Equipment used in testing.

Component	Measurement
Yokogawa 2531 Digital Power Meter	dc voltage, current, power
Tektronix TDS 3034B e*scope	Collect waveforms and data
Tektronix P5210 High Voltage Differential Probe	ac voltage
Tektronix A622 ac/dc Current Probe	ac current
Tektronix P5200 High Voltage Differential Probe	dc voltage
Tektronix TCP202 Current Probe	dc current

#### 1.4 TESTING PROCEDURE

Once test installation had been completed, the quantities to be recorded needed to be determined. On the ac side:

- Voltage and current fundamental period with rms values
- Lag between the voltage and current

On the dc side:

- Voltage and current average values

The following quantities will then be calculated:

- dc Power:  $P_{dc} = I_{dc}V_{dc}$
- ac power:  $P_{ac} = I_{ac}V_{ac}$
- Efficiency:  $\eta = \frac{P_{out}}{P_{in}} \times 100\% = \frac{P_{ac}}{P_{dc}} \times 100\%$
- Power factor:  $pf = \cos(\theta_i - \theta_v)$  Can then determine if leading or lagging.

Waveforms and data were captured by using a LAN connection from the scope to a computer. The local interface of the scope allowed waveforms to be captured by obtaining a screen shot of the scope.

## 1.5 RESULTS

Fig. 4 shows the fundamental periods for both the dc voltage and current and the ac voltage and current. Ch1 is the ac voltage and Ch2 is the ac current, with rms values of 207 V and 801 mA. Ch3 is the dc voltage and Ch4 is the dc current, with average values of 24.5 V and 7.04 A. It should be noted that the ac waveforms are at a fundamental frequency of 60 Hz and the dc waveforms have a ripple of two times the fundamental frequency. Fig. 5 shows the lag between the ac voltage and current. Ch1 is the ac voltage and Ch2 is the ac current. It can be seen that the ac current lags the ac voltage, with a phase difference of  $5.61^\circ$ .

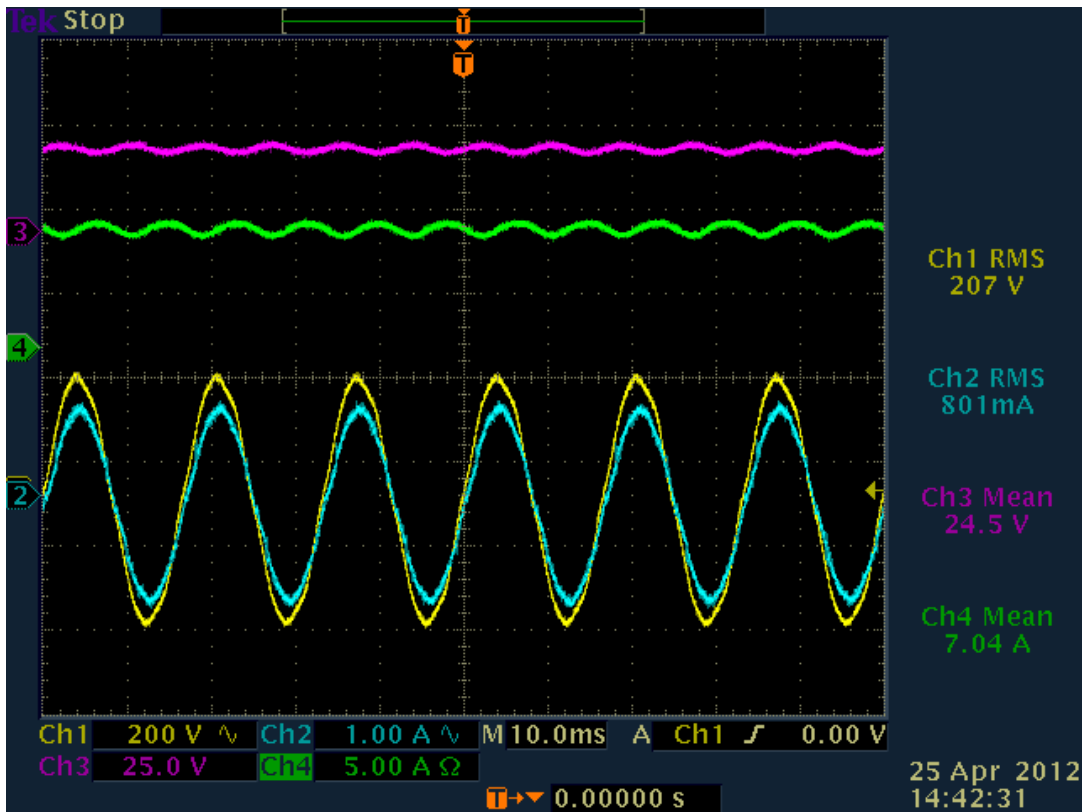


Fig. 4. Voltage and current waveforms.

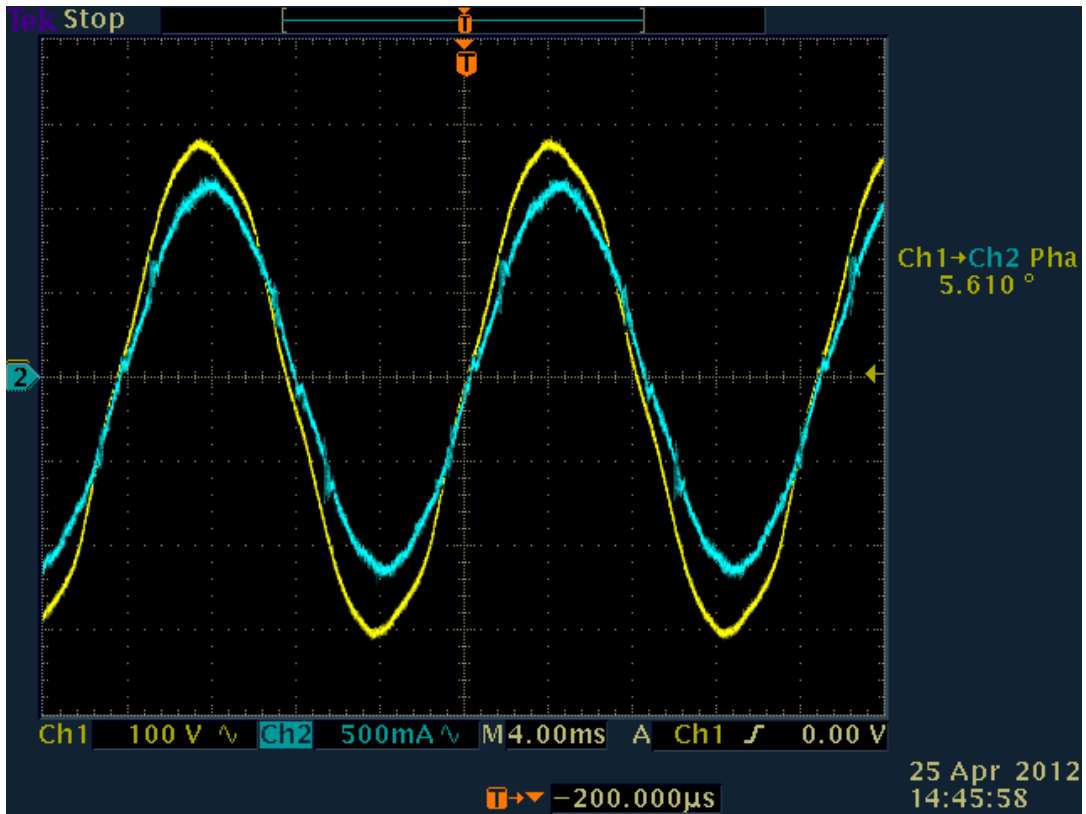


Fig. 5. Lag between ac voltage and current.

## 1.6 CALCULATIONS

Table II. Experimental results.

Measurement	Value
$V_{dc}$	24.5 V
$I_{dc}$	7.04 A
$v_{ac}$	207 V <sub>rms</sub>
$i_{ac}$	801 mA <sub>rms</sub>
$\Delta\theta$	5.61°

From Fig. 4,

$$P_{dc} = I_{dc}V_{dc} = (7.04 A)(24.5 V) = 172.48 W$$

$$P_{ac} = i_{ac}v_{ac} = (801 mA_{rms})(207 V_{rms}) = 165.81 W$$

$$\eta = \frac{P_{out}}{P_{in}} \times 100\% = \frac{P_{ac}}{P_{dc}} \times 100\% = \frac{165.81 W}{172.48 W} \times 100\% = 96.13 \%$$

From Fig. 5,

$$\Delta\theta = 5.61^\circ$$

$$pf = \cos(\theta_i - \theta_v) = \cos(5.61^\circ) = 0.995 \text{ lagging}$$

## 1.7 CONCLUSIONS

The quantities measured and values calculated were in agreement with the manufacturer's specifications. From the calculations, the peak efficiency of the Enphase M190 Microinverter is 96.13 %, which is approximately the stated value of 95.5 %. Slight errors in measurements can account for this, but further testing over longer periods of time should be done in order to more accurately measure the efficiency of the device. Future work could also involve calculating the CEC weighted efficiency of the device. The power factor was found to be 0.995 lagging, which is in agreement with the claim that the power factor is >0.95 lagging. From the data gathered, it can be seen that microinverters are viable options when it comes to converting dc power into ac power. However, improvements in microinverter technology can still be made in order to decrease the cost of these devices so that they can better compete with other conventional energy sources.

## CHAPTER 2: IRRADIANCE DATA LOGGING

### 2.1 INTRODUCTION

As the use of solar energy becomes increasingly more popular, the need to improve on solar power technology is becoming more necessary. The developments of new technologies such as the microinverter have made solar power an increasingly viable producer of power. However, rapid fluctuations in the output of PV modules and solar energy systems due to shading and other factors adherent to specific geographical locations can potentially slow progress towards integrating PV power systems. In order to consider the geographical and climatic effects on PV sites, irradiance data needs to be collected and analyzed. Irradiance is the power per square meter that is incident to a surface, in the case of PV systems, the surface of a PV panel. By collecting this data, it is possible to understand the severity in which solar insolation can fluctuate at a single site. By knowing and analyzing irradiance data at multiple PV sites, it can then be possible to determine which PV sites to utilize and combine in order to minimize the fluctuations in power output [2]. The objective of this work is to measure and log irradiance data at a frequency of 1 Hz, or one measurement every second, which is considerably higher frequency when compared to measurements taken, for example, every fifteen minutes [3]. This work consists of measuring the irradiance with a pyranometer, and using a data acquisition system to log the measurements, shown in Fig. 6.

The pyranometer used is an Apogee SP-215 5V amplifier model. The output of the pyranometer is a voltage with a range of 0.0 V to 5.0 V. Irradiance can then be calculated using the manufacturer's calibrated conversion factor of  $0.25 \text{ Wm}^{-2}$  per mV. According to the manufacturer, full sunlight should be a voltage output of approximately 4.4 V, which is 1100

$Wm^{-2}$  [4]. The data acquisition system used is a National Instruments USB-6259 system with a program created in LabVIEW, NI's application software, to control the frequency of data collection and data file output. The following will include an outline of testing installation, including installation of the pyranometer and the DAQ system, and the procedure in which the data was collected. Experimental results and analyses will then be presented, followed by conclusions made about the data collected.

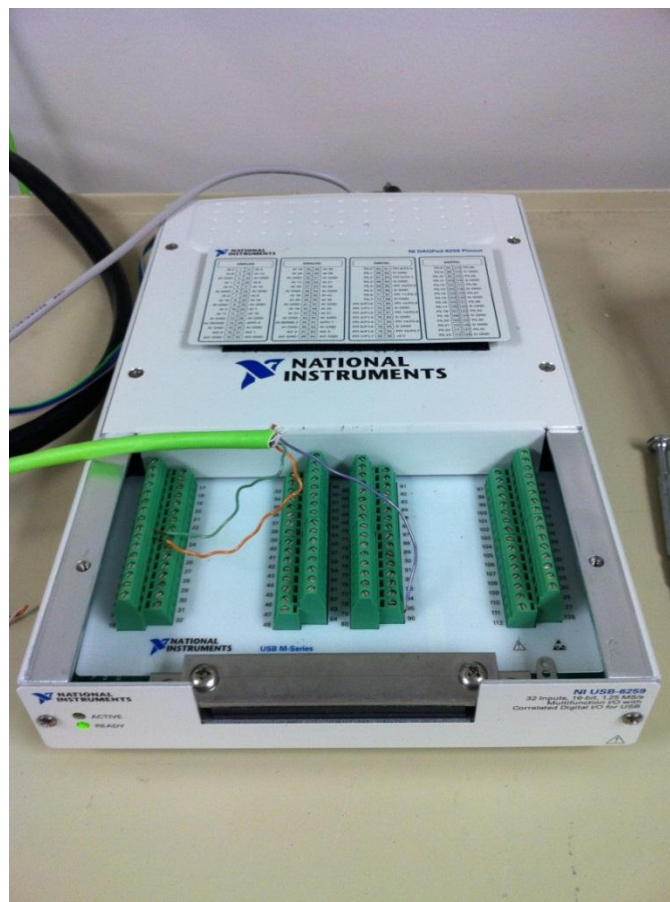


Fig. 6. NI USB-6259 DAQ system.

## 2.2 TESTING INSTALLATION

Testing began by installing the Apogee SP-215 pyranometer on top of the Engineering Hall roof near the site of the PV panels. It was installed at a  $66^\circ$  angle, which is on the same plane as the panels. The cable from the pyranometer was pulled through the same conduit and junction box as the PV panels, and wired to the NI USB-6259 data acquisition system. Fig. 7 shows how the pyranometer is wired to the DAQ system. There are three conductors in the pyranometer cable, one for the 5 V input power (purple), one for the signal from the sensor (green), and the other for ground (orange). The sensor signal is wired to Pin 8 and ground is wired to Pin 9. These specific pins were designated by LabVIEW's DAQ Assistant in order to acquire a voltage measurement. The DAQ Assistant will be discussed further under the section DAQ ASSISTANT. The 5 V input power conductor was wired to Pin 96 of the NI USB-6259, which is a +5 V power source that is built in to the DAQ system. The DAQ system is connected to a computer through a USB connection and configured through LabVIEW.

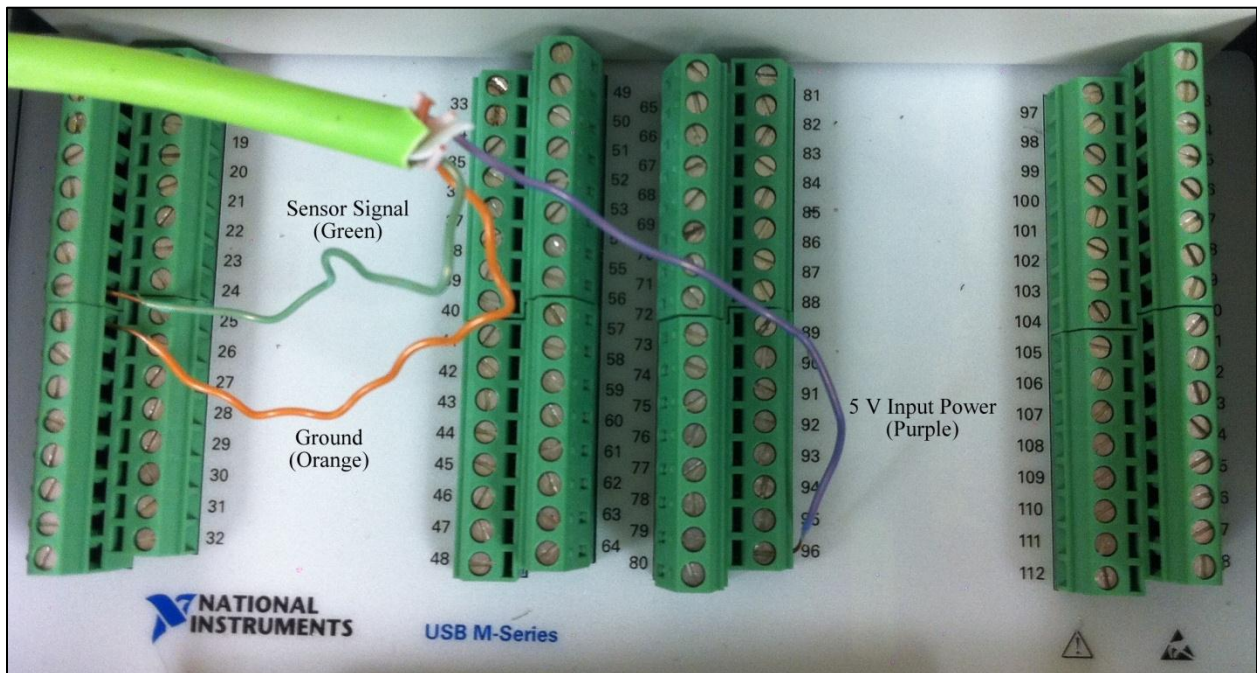


Fig. 7. Pyranometer conductor connections.



## 2.3 DAQ ASSISTANT

LabVIEW is NI's application development platform for test and measurement automation. It is graphically based and consists of designing a VI, or virtual instrument, with graphical blocks in order to acquire and save data without programming. For National Instrument devices, LabVIEW has a data acquisition assistant block, titled DAQ Assistant, which simplifies measuring and logging data. To begin designing the VI to collect and log the irradiance data, the DAQ Assistant block was placed in the VI and configured to measure the voltage output from the pyranometer.

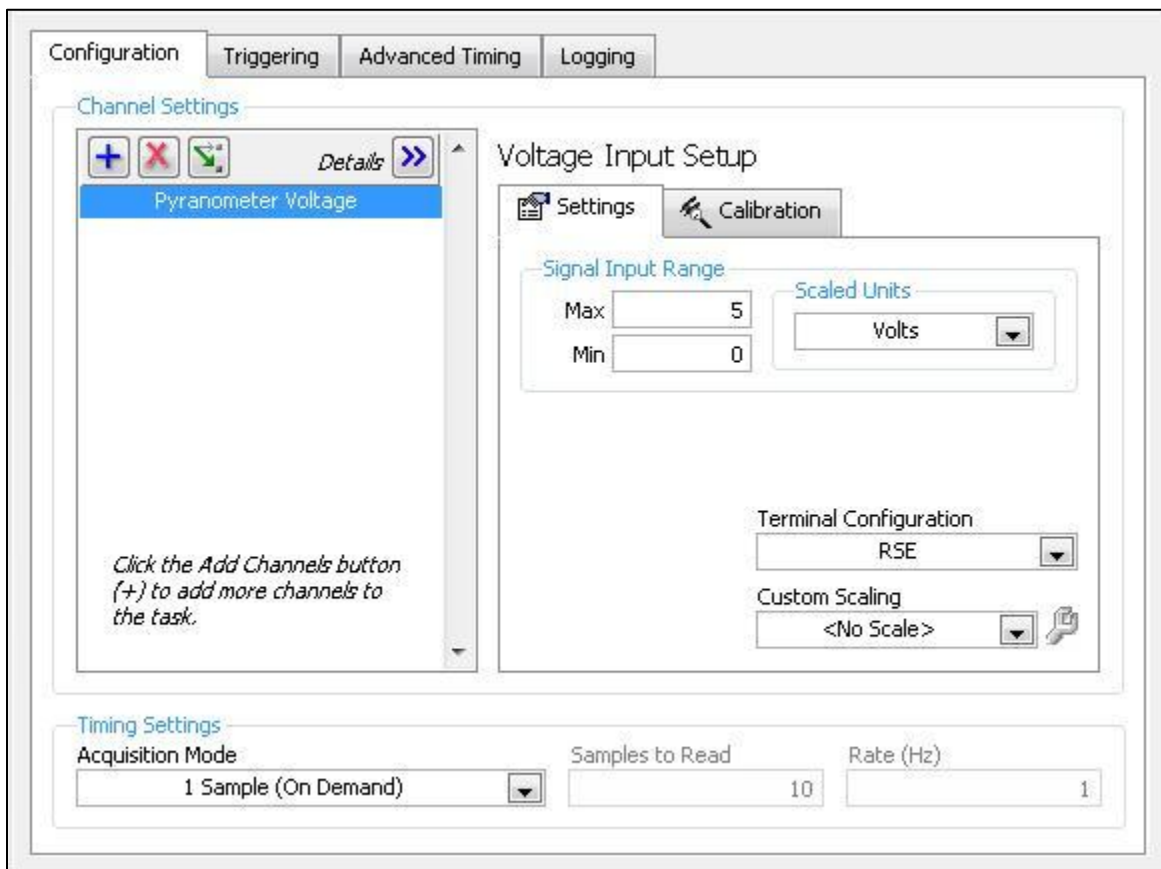


Fig. 8. DAQ Assistant configuration menu.

Fig. 8 shows the menu for the DAQ Assistant block and the settings that were chosen. The channel named Pyranometer Voltage was configured to acquire an analog voltage with a signal input range of 0 V to 5 V. The acquisition mode was set to 1 Sample (On Demand) in order to measure one sample per iteration of a one second timing loop. The DAQ Assistant also shows the connection diagram for connecting the input wires to the DAQ system. As seen in Fig. 9, the output signal of the sensor (CH+) was wired to Pin 8 and ground (CH-) was wired to Pin 9.

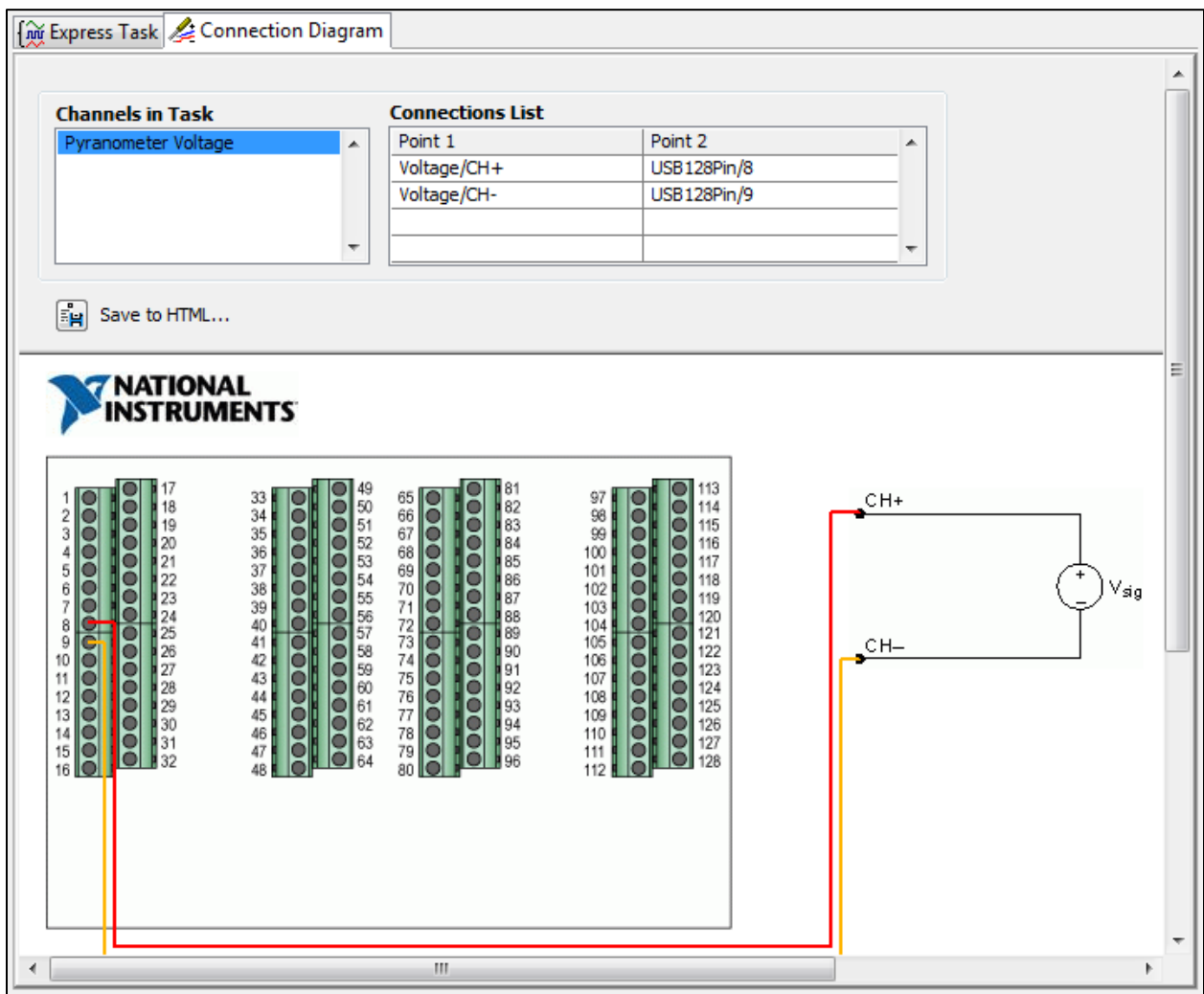


Fig. 9. DAQ Assistant connection diagram.

## 2.4 LABVIEW VI

The following section is a run through of the LabVIEW VI. The name of the VI is PV\_data\_logging\_NI\_USB6259.vi. To begin data collection, the VI has to be manually started. Once it begins to run, a time stamp is generated, along with the file name and location. The LabVIEW code for this section is presented below in Fig. 10. The format in which the file is named is “senior\_design\_pv\_data\_date\_%m\_%d\_%Y\_time\_%H\_%M\_%S.csv”. For example, if the time and date was 1:00 pm on August 1, 2011, the file name would be “senior\_design\_pv\_data\_date\_08\_01\_2011\_time\_13\_00\_00.csv”. After the file name is generated, the file path is built. The location to where the file will be saved is on the local computer hard drive. Once the file name and location is generated, headers are written into the opened file. The LabVIEW code for this section is presented below in Fig. 11. The file headers are written into the file as the first line of text, with commas as the delimiter. The header of a file would read “Year, Month, Day, Hour, Minute, Second, Voltage”.

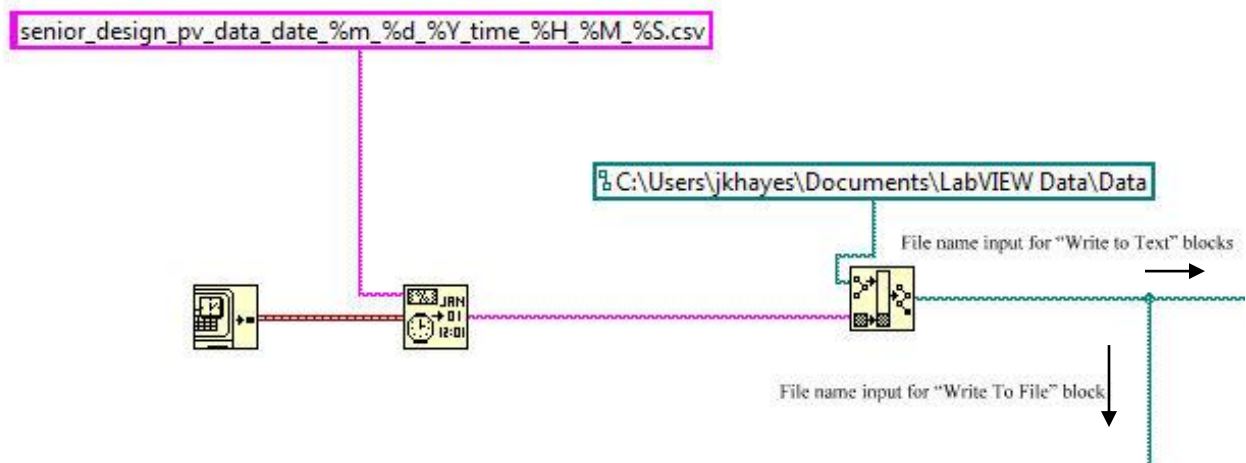


Fig. 10. Data file name and location.

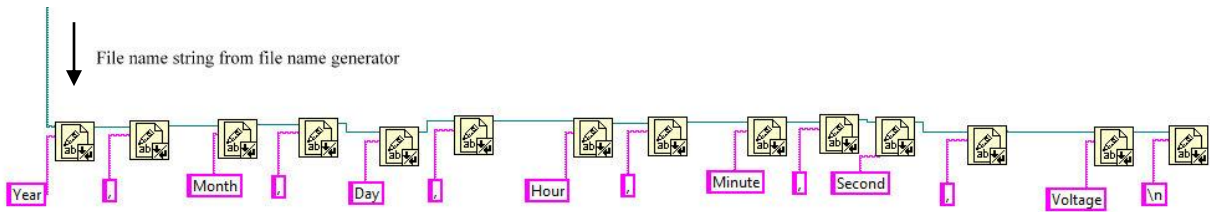


Fig. 11. File headers.

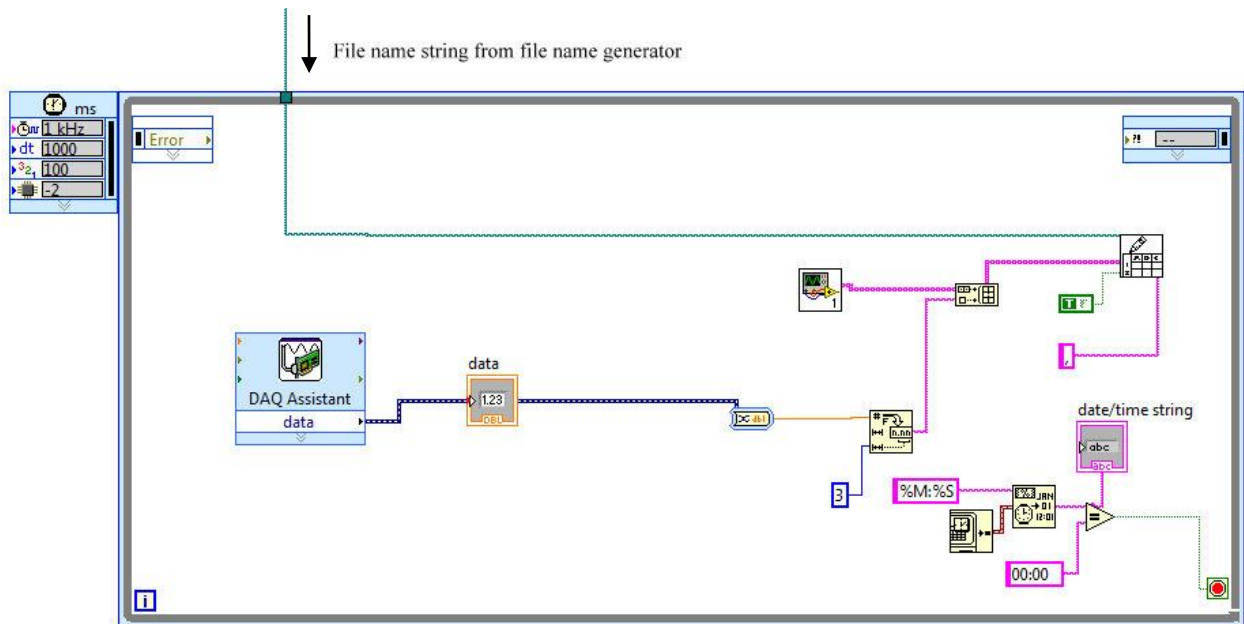


Fig. 12. Timing Loop.

Once the file name, location, and headers are generated, the data logging begins. A one second timing loop was placed around the DAQ Assistant block and Write-to-File block. This allows the DAQ Assistant to collect a sample every second and write the sample data to the generated file. Since the DAQ Assistant was configured to run on demand, the DAQ Assistant measures the pyranometer voltage every second, or every loop iteration. While the DAQ Assistant is taking a measurement, a time stamp is generated so as to know the precise second that the measurement is taken. The time stamp is generated and converted to a string array in the same format and order as the headers. The voltage measurement taken by the DAQ Assistant is then converted to a string and added to the array. The array is then written to the file that was generated when the VI first began. The timing loop will continue until the hour and minute

become 00:00. This is in order to close the opened file and create a new file at the beginning of each hour. A Boolean equation was created that simply states that if the minutes and seconds equal 00:00, then stop the timing loop. Once the timing loop ends, the entire process will restart due to a while loop around the entire VI. This causes the VI to continuous run until it is manually stopped.

## 2.5 RESULTS

After converting the pyranometer voltage measurements recorded by the DAQ system into irradiance measurements using the conversion factor of  $0.25 \text{ Wm}^{-2}$  per mV, the data is very consistent with the theoretical irradiance values that would be expected at the location of the pyranometer. Apogee Instruments provides an online irradiance calculator, Clear Sky Calculator, which calculates the theoretical irradiance values, expected with a clear sky at a certain geographical location [4]. When looking at the effects of geographical characteristics, the data shows how much cloud cover or shading can affect irradiance levels, thus affecting the output of the PV system. Fig. 13 shows irradiance data gathered between August 1, 2011 and August 8, 2011. Fig. 14 shows one day's worth of irradiance data collected on August 5, 2011. Both of these figures show the intermittency problem of irradiance and PV power. As seen in Fig. 14, the first part of the day was cloudless or no major shading occurred, providing a nice irradiance profile. However, major fluctuations and rapid change in irradiance levels began to occur very often later that day. This would lead to rapid fluctuations in the maximum output power of a PV system, creating some unreliability and decreasing the power quality.

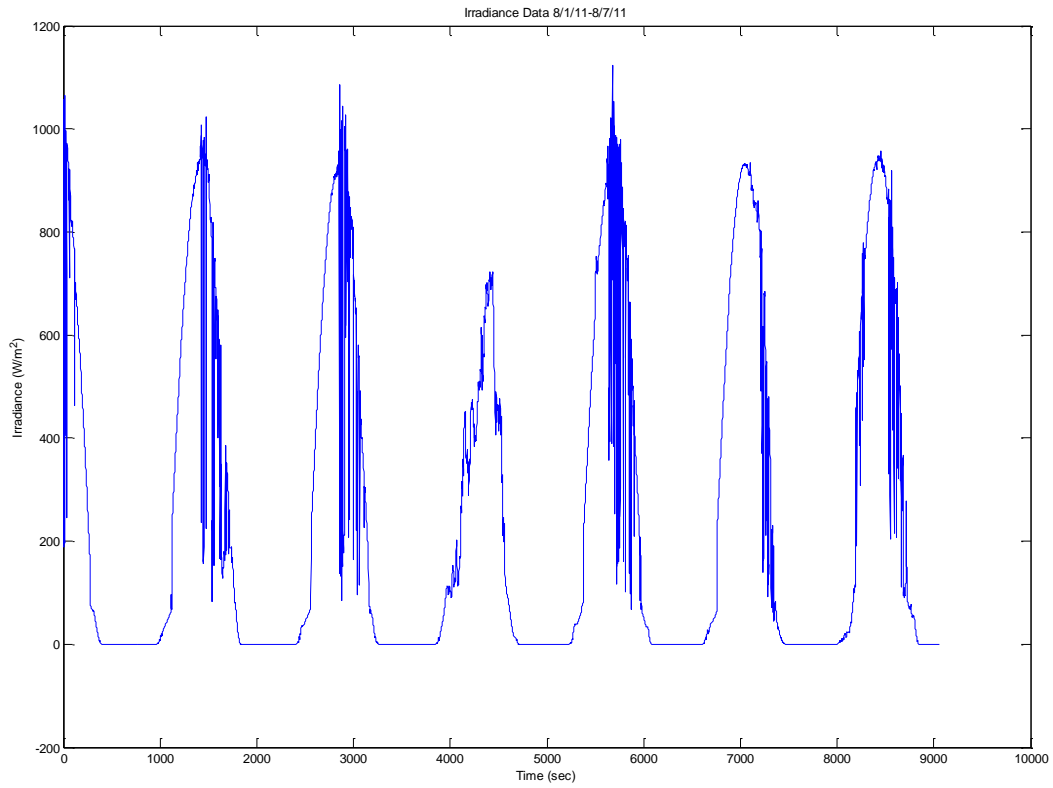


Fig. 13. Irradiance data from 8/1/2011 to 8/7/2011.

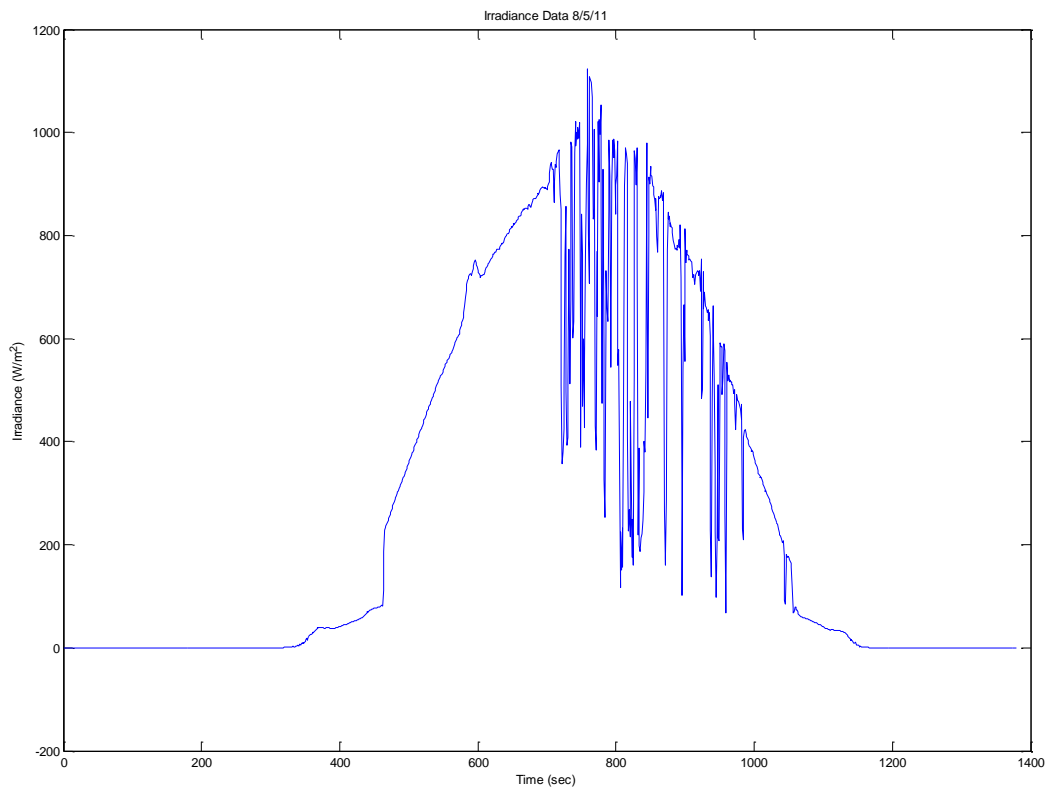


Fig. 14. Irradiance data from 8/5/11.

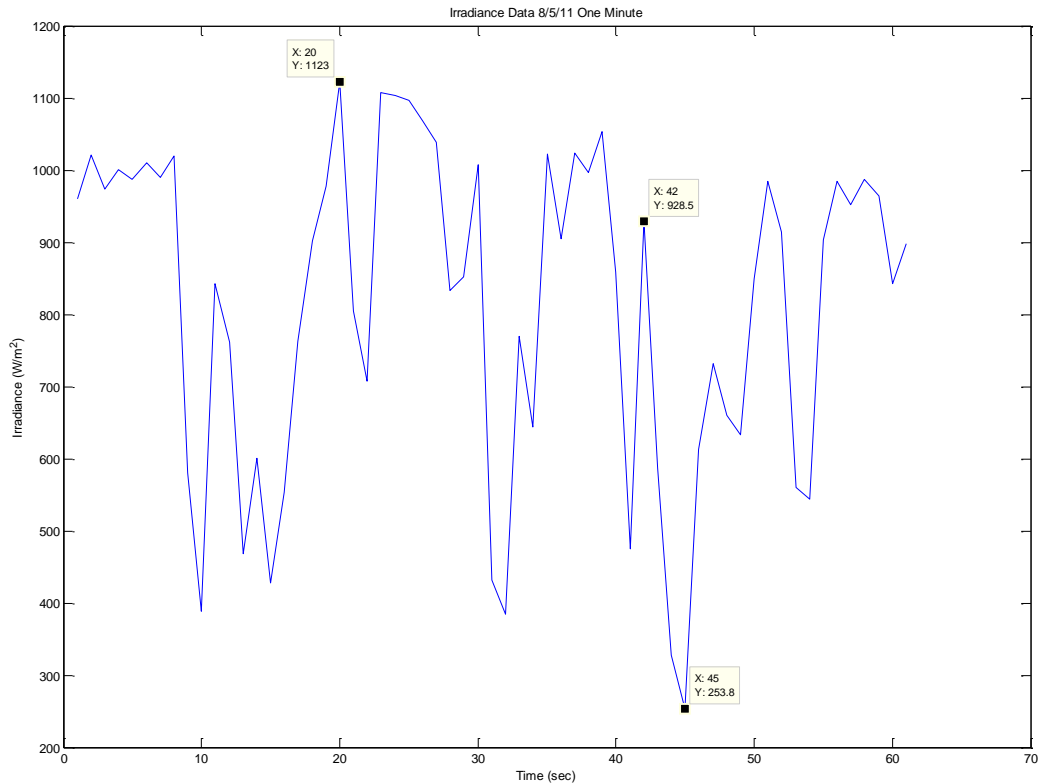


Fig. 15. Irradiance data from 8/5/11 (one minute).

Fig. 15 further zooms in on the irradiance data collected on August 5, 2011. The plot shows 60 seconds worth of data. The major fluctuations in irradiance can now be seen. From the figure, the maximum irradiance value during this period is  $1123 \text{ Wm}^{-2}$ . The lowest value is  $253.8 \text{ Wm}^{-2}$ . It can be seen that this minimum occurs after a drop in irradiance from  $928.5 \text{ Wm}^{-2}$  to  $253.8 \text{ Wm}^{-2}$  in only 3 seconds, once again display how intermittency can cause problems.

## 2.6 CONCLUSIONS

From the data collected, it can be seen that the fluctuations in PV output can be cause for concern. If a decrease in solar insolation means a decrease in output power, then a system with many fluctuations can cause poor power quality and reliability [4]. However, generalizations about utility-scale PV intermittency cannot be made from this data. This data represents a single

point of solar insolation, whereas a PV panel and a utility-scale system will provide a greater surface area of insolation, potentially smoothing out the fluctuations in output power [2].



## CHAPTER 3: IMPACT OF PV ON VOLTAGE REGULATION

### 3.1 INTRODUCTION

As previously stated, there is a rapid trend towards utilizing the benefits of alternative energy sources such as solar power. With this increased trend, comes more photovoltaic distributed generation (PVDG). Higher levels of PV penetration can have certain positive effects on current distribution systems, including the increased use of conservative voltage regulation (CVR). CVR is the practice of lowering the substation voltage in order to reduce the load power demand on the distribution system. Estimates have shown that for an average substation voltage decrease of one-percent, there is also a decrease in the load demand by one-percent [6]. The effects that a high penetration of PVDG can have on voltage regulation and CVR can be understood with computer simulations. The following work uses a distribution feeder model to illustrate the effect of PVDG on voltage regulation.

### 3.2 DISTRIBUTION FEEDER MODEL

The distribution feeder under analysis has parameters as shown below in Table III and Table IV. It is a radial three-phase distribution feeder with a nominal line-to-line voltage of 13.8 kV. Bus 1 is an infinite bus and Bus 2 is the primary side of the transformer. The three-phase transformer steps down the voltage from 115 kV to 13.8 kV and has a rating of 20 MVA. The transformer equivalent impedance is  $0.62 + j8.91$  % of the transformer base impedance. The three-phase short circuit current at the primary side of the transformer is 8952 A. Fig. 16 shows the calculations made in order to model the feeder, which is shown in the Appendix.

Table III. Feeder impedances.

From (Bus)	To (Bus)	R ( $\Omega$ )	X( $\Omega$ )
3	4	0.29	0.62
4	5	0.17	0.35
5	6	0.09	0.19
6	7	0.42	0.90
7	8	0.22	0.47
8	9	0.96	0.78
9	10	0.63	0.51
10	11	0.90	0.73

Table IV. Bus Peak Loads.

Bus	P (kW)	Q <sub>lag</sub> (kVAr)
3	600	300
4	500	250
5	450	180
6	1500	600
7	1800	1100
8	840	500
9	500	220
10	300	150
11	150	100

```

feeder = struct();
feeder.Sb = 20e6;
feeder.Vb = 13.8e3;
feeder.Zb = (feeder.Vb)^2/(feeder.Sb);

zxf = (0.62 + 1j*8.91); % distribution transformer impedance in pu
Zxf = feeder.Zb*zxf/100; % distribution transformer impedance in si
Rxf = real(Zxf);
Xxf = imag(Zxf);

Isc = 8952;
absZsc = feeder.Vb/(sqrt(3)*Isc); % infinite bus short-circuit impedance
Xsc = sqrt(absZsc^2 - Rxf^2) - Xxf;

feeder.branch.nf = 1:10;
feeder.branch.nt = 2:11;
feeder.branch.R = [0 real(Zxf) .29 .17 .09 .42 .22 .96 .63 .9]';
feeder.branch.X = (1/377)*[Xsc imag(Zxf) .62 .35 .19 .9 .47 .78 .51 .73]';
feeder.bus.P = [0 0 600 500 450 1500 1800 840 500 300 150]'*1e3;
feeder.bus.Q = [0 0 300 250 180 600 1100 500 220 150 100]'*1e3;

```

Fig. 16. Parameter calculations.

### 3.3 RESULTS

The simulations were run at peak loading conditions to see the effects that a high penetration of PVDG can have under the worst conditions. The first simulation was done without any PVDG. Fig. 17 shows the bus voltages and Fig. 18 shows the bus voltages in per-unit, using a base of 13.8 kV. Considering  $\pm 5\%$  of the substation voltage to be an acceptable voltage range for the feeder, the results of the simulation as seen in Fig. 18 show that the voltages of Bus 6 through Bus 11 fall below 0.95 pu. Therefore, the voltage at the substation was increased to 1.03 pu. The results of this simulation can be seen in Fig. 19. From Fig. 19, all of the bus voltages are now above the acceptable voltage level of 0.95 pu.

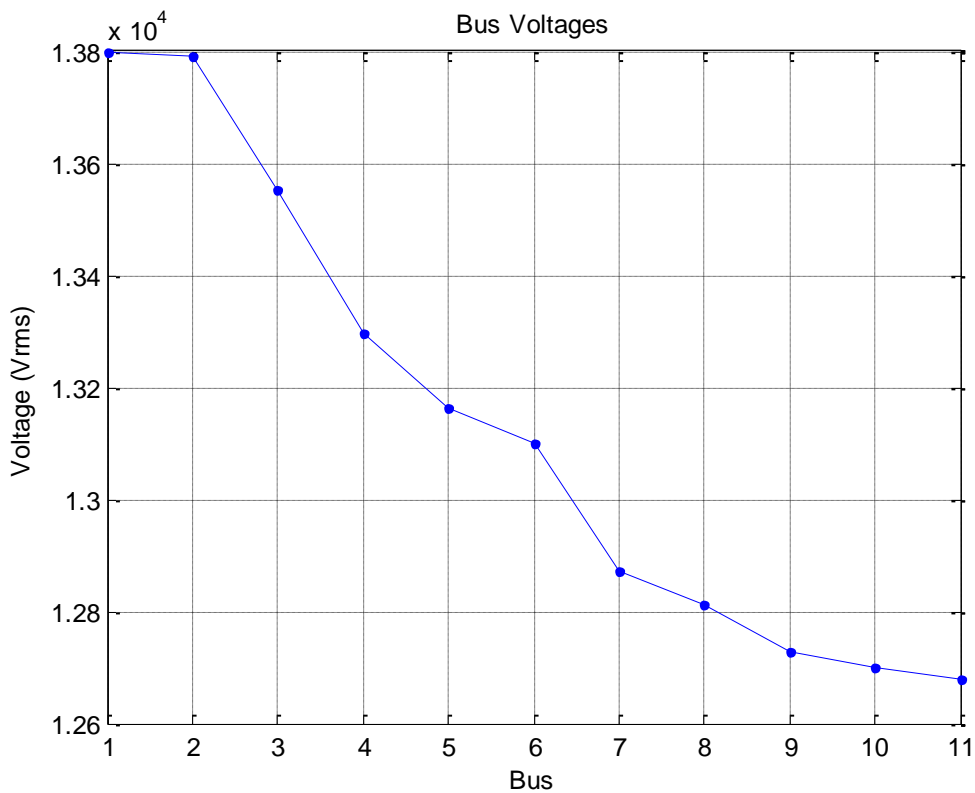


Fig. 17 Bus voltages with substation voltage at 1 pu.

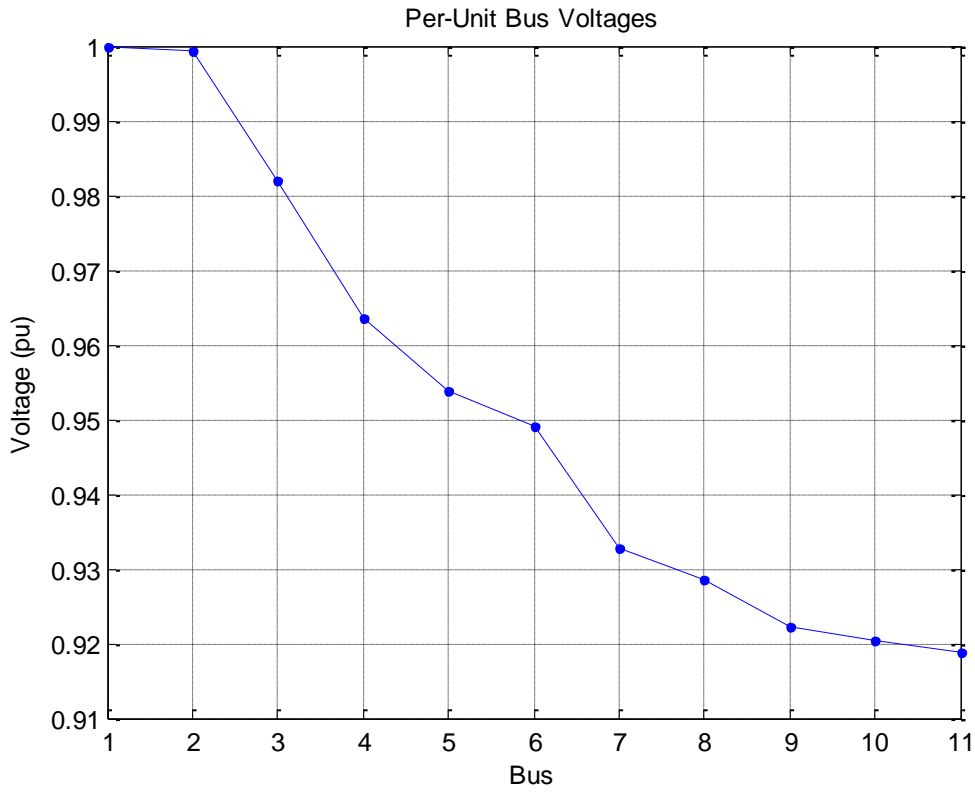


Fig. 18. Per-unit bus voltages with substation voltage at 1 pu.

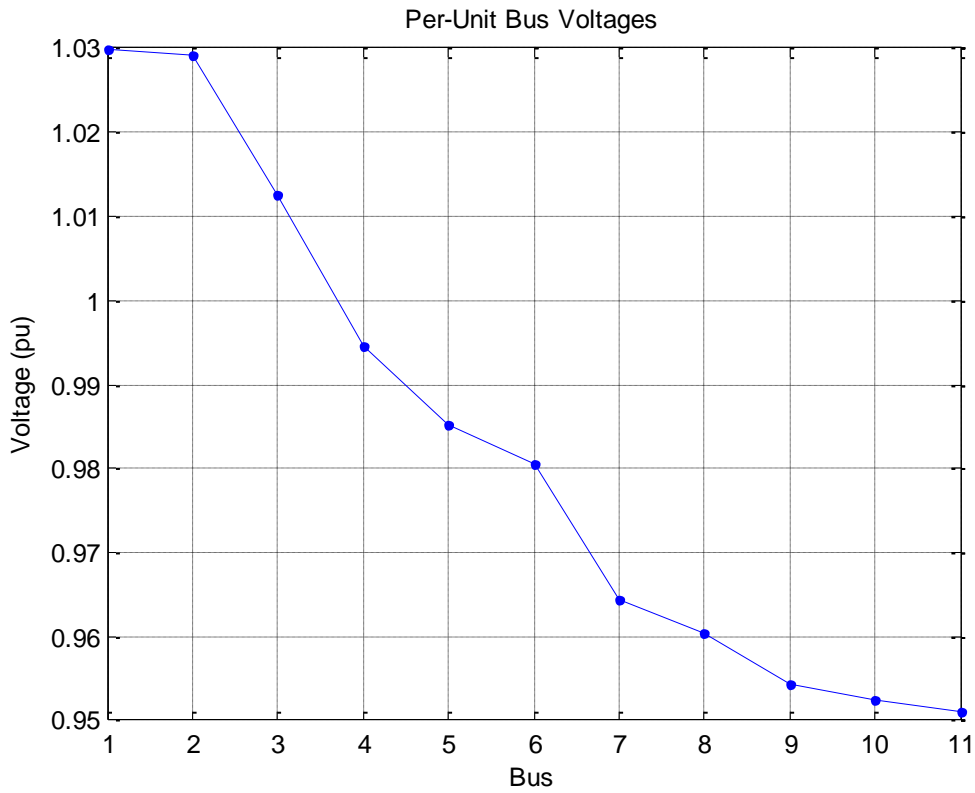


Fig. 19. Per-unit bus voltages with substation voltage at 1.03 pu.

Now that the voltage levels are in the acceptable range, the effects of PV penetration can be seen and utilized in order to implement CVR. The PVDG was placed at the end of the feeder since the lowest voltage in the feeder occurs at the end. Other factors such as size, cost effectiveness or placement were not considered. The PV data shown in Fig. 14 was used for the simulation. A correlation of one-to-one was used so that, for example,  $1100 \text{ Wm}^{-2}$  would correspond to 1100 W of PV power being injected into the system. Fig. 20 shows this relationship. This power was injected into the system using a three-phase dynamic load. Therefore, the power was multiplied by a factor of -1 so that the dynamic load would inject power. The PV data was also multiplied by a factor of 1000 in order to increase the max PV power to approximately 1.2 MW, which simulates a large PV farm. Fig. 21 shows this injected power.

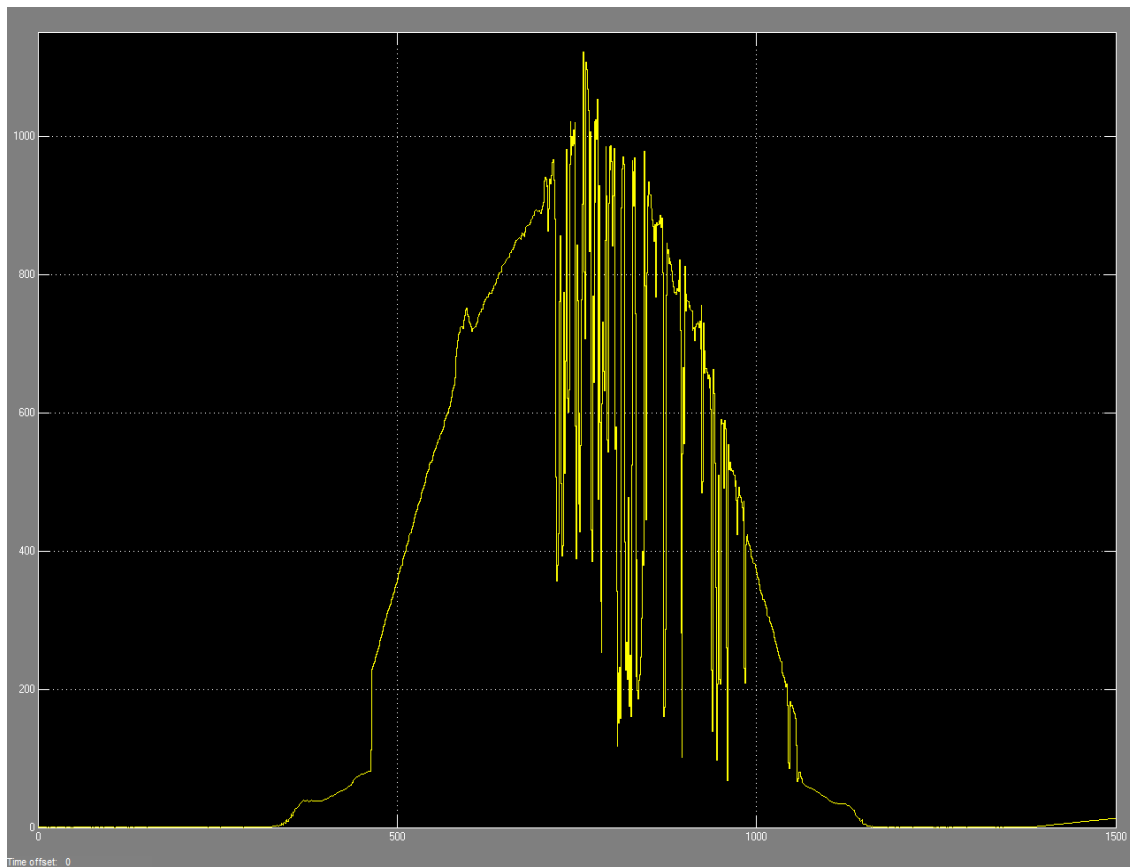


Fig. 20. PV power taken from irradiance data.

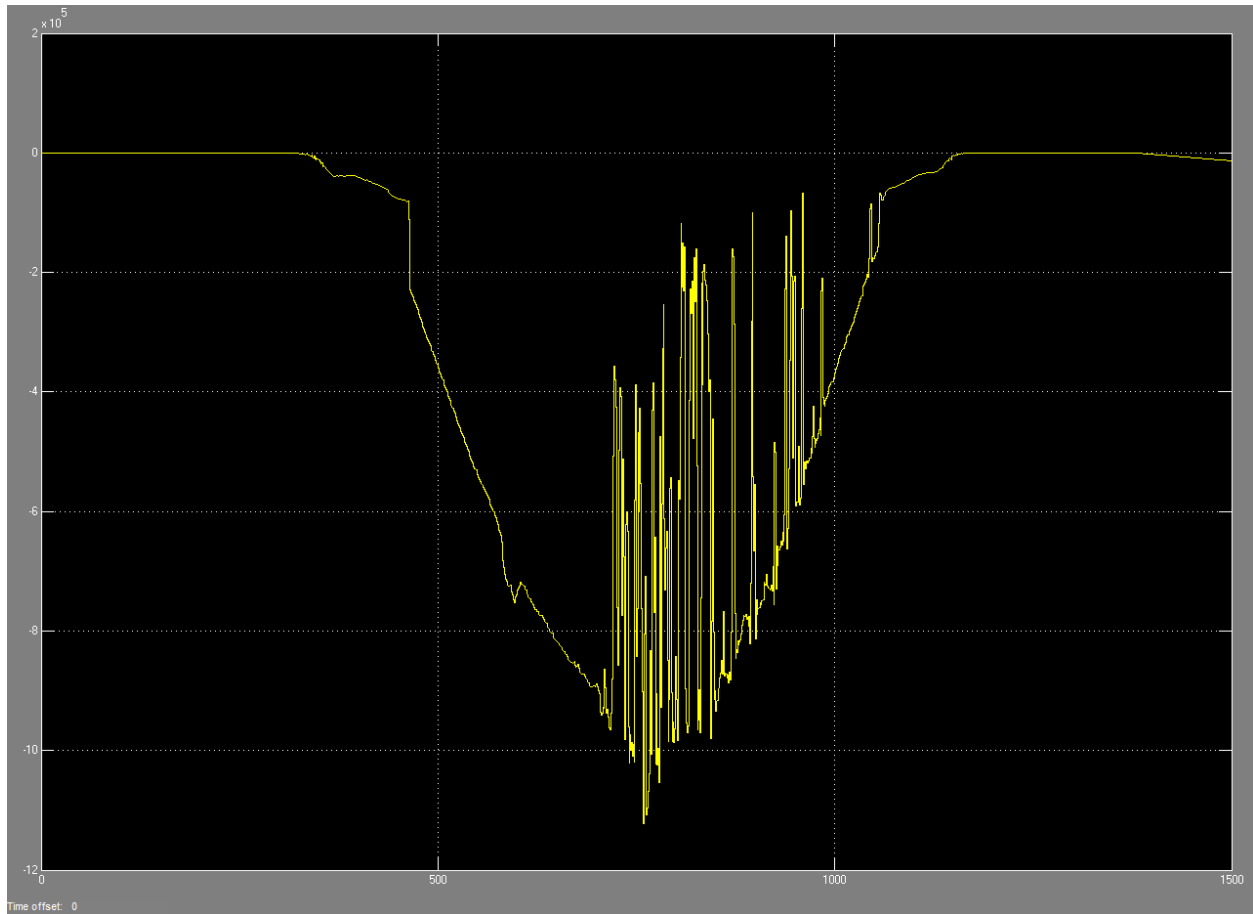


Fig. 21. Injected PV power.

Now with the injected PV power set to an appropriate level, the simulation was run with the same settings as the previous simulation. Fig. 22 shows the results. It can be seen that the injected PV power increased the voltage levels on the buses towards the end of the feeder and provide a greater margin above the lower limit of 0.95 pu. Now that the voltage levels are higher, CVR can be implemented in order to reduce the substation voltage and reduce the overall demand. The voltage at the substation was lowered to 1.025 pu. From Fig. 23 with the added PV, the voltage levels at the end of the feeder are still above 0.95 pu and thus within the acceptable voltage range; therefore utilizing CVR and in turn, lowering the demand on the system.

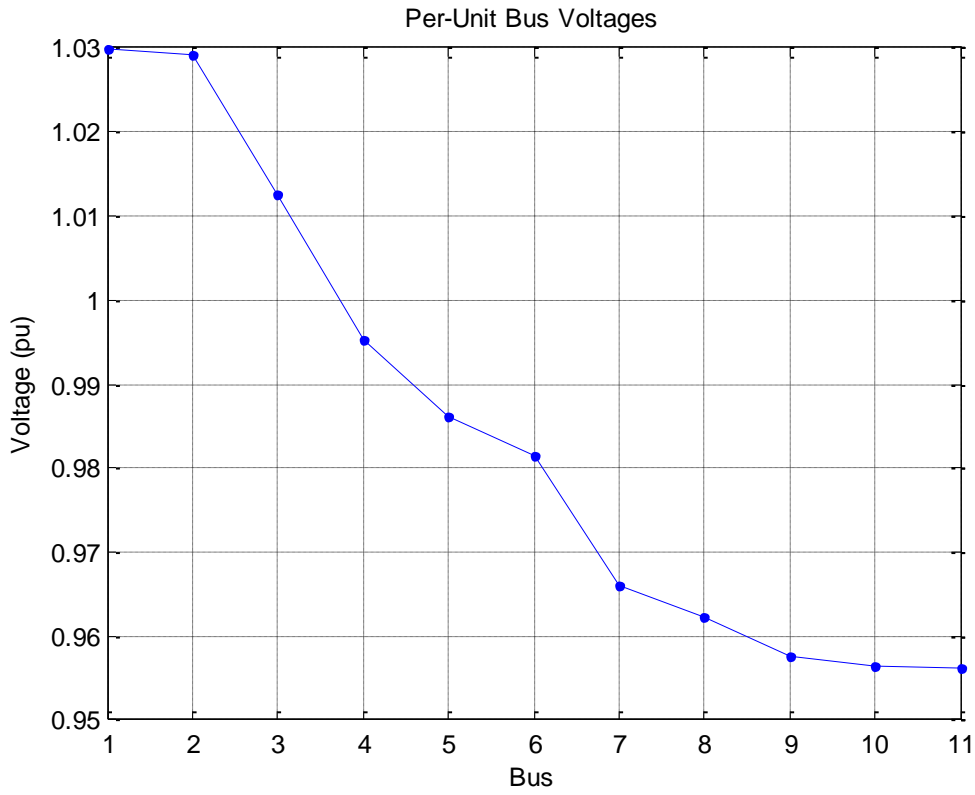


Fig. 22. Per-unit bus voltages with substation voltage at 1.03 pu and PVDG at bus 11.

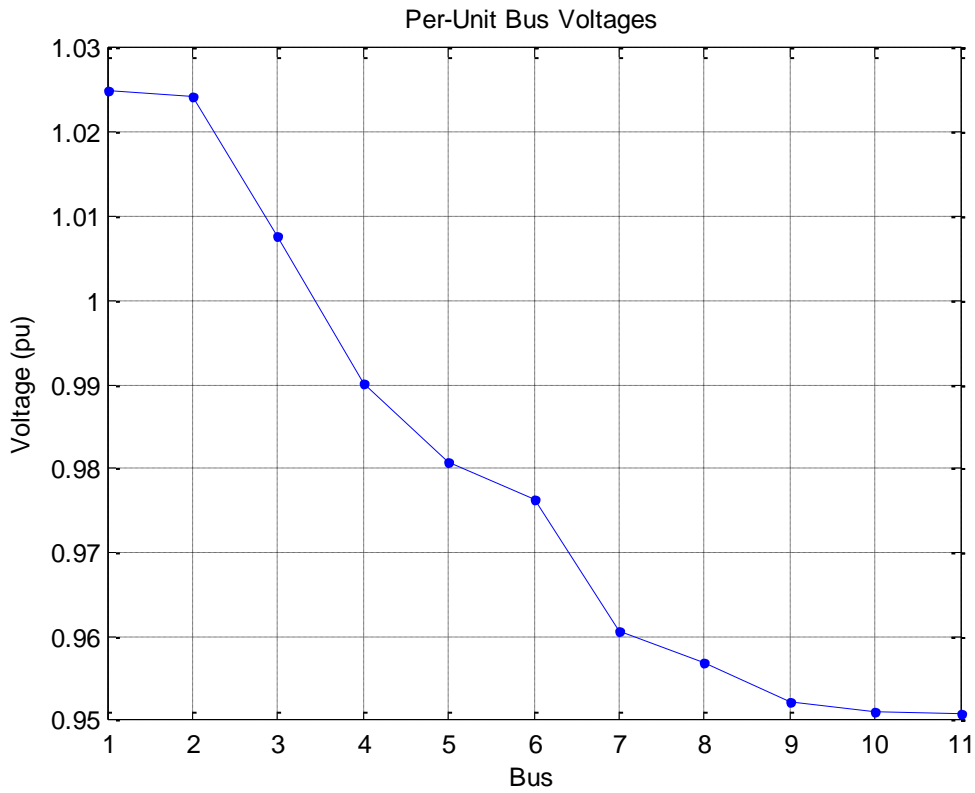


Fig. 23. Per-unit bus voltages with substation voltage at 1.025 pu and PVDG at bus 11.

### 3.4 CONCLUSIONS

While this is just one isolated case, the work shows that PVDG can have a significant impact on current distribution systems. However, other factors not included in this analysis should be included in future work. There are limitations, such as placement and sizing of the PVDG along the feeder, and cost-effectiveness that should be considered when implementing a PVDG system. Other technology such as energy storage units or smart PV inverters can be implemented into the system as well to create a more efficient system. However, there is no denying the fact that PVDG can add many benefits to a distribution system.



## REFERENCES

- [1] “Enphase M190 Datasheet,” Enphase Energy, 2011.
- [2] A. Mills and R. Wiser, “Spatial and Temporal Scales of Solar Variability: Implications for Grid Integration of Utility-Scale Photovoltaic Plants,” *uwig.org*. [Online]. Available: <http://www.uwig.org/pvwork/11-Mills-GeographicDiversityAndPV.pdf>. [Accessed Aug. 1, 2011].
- [3] Florida Solar Energy Center, “Inverter Testing for PV Systems,” *Florida Solar Energy Center*. [Online]. Available: <http://www.fsec.ucf.edu/en/research/photovoltaics/inverter/index.htm>. [Accessed Aug. 14, 2011].
- [4] Apogee Instruments, “Amplified Pyranometer SP-212 & 215,” *apogeeinstruments.com*. [Online]. Available: [http://www.apogeeinstruments.com/manuals/SP-212\\_215manual.pdf](http://www.apogeeinstruments.com/manuals/SP-212_215manual.pdf). [Accessed July 21, 2011].
- [5] J. Apt and A. Curtright, “The Character of Power Output from Utility-Scale Photovoltaic Systems,” *cmu.edu/electricity*. [Online]. Available: [http://wpweb2.tepper.cmu.edu/ceic/PDFS/CEIC\\_07\\_05\\_lvu.pdf](http://wpweb2.tepper.cmu.edu/ceic/PDFS/CEIC_07_05_lvu.pdf). [Accessed Aug. 2, 2011].
- [6] C. A. McCarthy and J. Josken, “Applying capacitors to maximize benefits of conservation voltage reduction,” in *Rural Electric Power Conference, 2003*, 2003, p. C4–1 – C4–5.

# APPENDIX

## Distribution Feeder Model

